Report on TIDAL Network Plus Feasibility Project:

Algorithmic design of functionally graded prosthetic liners

Authors

Ben Oldfrey, UCL

Alex Dickinson, University of Southampton

Elze Porte, UCL

Laurence Russell, University of Southampton

Christian Partik, UCL

Acknowledgements

This project was funded by the Engineering and Physical Sciences Research Council [grant number: EP/W00717/1] through TIDAL Network Plus - Transformative Innovation in the Delivery of Assisted Living Products and Services.

What we set out to discover

Background and research context

Additive manufacturing now allows multi-material and structurally complex composite products that could not previously be created. This unlocks our ability to replicate many advantageous structures found in biological tissues.

Nature creates incredible interfacing mediums between hard and soft materials in the body by gradation of connecting tissues. This spreads the stresses being translated through, for example tendons and ligaments, rather than concentrating stress at specific points, increasing damage tolerance.

Stress management and comfort at the prosthetic socket interface is an ongoing challenge, in particular combating shear stresses. While graded stress profiles at the stump socket interface could inherently reduce wear and improve component life spans and therefore improving the sustainability of devices, complex composite material structures are in opposition to design guidelines that facilitate material recovery and standard sustainability strategies.

New repairability or life-prolonging strategies must be devised for these structures, such as the re-application of soft layers to maintain surface integrity or to protect emergent sites of local tissue sensitivity or vulnerability.

Th work builds on materials development work at UCL on soft material structures, and predictive socket design and modelling work at University of Southampton (and the spin out company Radii Devices).

Engineering / research challenge and why it matters

Over one billion people need one or more assistive devices, with a projected two billion in need by 2050 [1]. At the same time, global demand for resources at large is projected to double by 2050, all the while the climate crisis rages on [2].

In P&O, the use of digital manufacturing is rapidly accelerating, however is still focused on rigid material prosthetic componentry. Soft Elastomeric liners are commonly worn between socket and limb. This is due to their superior skin adhesion, load distribution and ability to form a seal [3]. Laboratory tests suggest that elastomeric liners allow reduced shear stress on the skin and give a higher cushioning effect on bony prominences, since they are soft in compression, and can be compliance-matched to biological tissues [5].

Due to the discrete nature of AM, it has been proposed as an effective approach to fabricate geometrically complex components such as functionally graded materials with optimized stress profiles and excellent formability, with concomitant environmental benefits, due to very limited material wastage.

It has been proposed that finite element analysis can complement clinical decision making for the appropriate design and manufacture of prosthetic sockets for amputees [6,7].

Repair is already highly problematic, yet ill-considered in provision models in many settings, although critical to useful product life span [2]. If, as expected, digital fabrication continues to drastically change the way P&O are produced, newly applicable repair strategies are essential.

Aims and objectives for the project

The aim of this project is to model and produce new functionally graded material interfaces for the improved comfort at the socket interface, along with developing repair strategies to match these advanced manufacturing techniques.

The objectives were:

1. Fabricate a set of novel graded patches of liner material

2. Model the socket interface with respect to optimising the stress profile through these soft materials

3. Develop a device level custom testing liner implementing these developments

4. Develop a repair and maintenance technique appropriate to these material structures

What we did

Material Testing

We tested compressive material properties of four commercially available elastomers: Ecoflex 00-10 (Smooth-On, Inc.), Ecoflex 00-30 (Smooth-On, Inc.), Dragon Skin 10 (Medium, Smooth-On, Inc.) and Smooth-Sil 950 (Smooth-On, Inc.). Ecoflex 00-10, Ecoflex 00-30 and Dragon Skin 10 were prepared by mixing part A and B in a 1:1 ratio, and Smooth-Sil 950 in a 10:1 ratio (A:B). The elastomers were thoroughly hand mixed and degassed in a vacuum chamber (Vevor, 1.5 gallon). Samples for testing were prepared in aluminium moulds of 28.6 mm diameter and 12.5 mm thickness (ASTM 575-91, example shown in Figure 1). Excess elastomer was removed with a flat metal scraper to level the samples. All samples were cured at room temperature. The thickness of the samples was found by taking the average of three measurements with a calliper at different locations on the sample.

Composite samples were prepared in two layers with Ecoflex 00-10 and Ecoflex 00-30. The same elastomer preparation method and sample moulds were used as for the single material samples. A small amount of dye (<1%, Silc Pig, Smooth-on, Inc) was added to the elastomers to distinguish the layers. The first layer was created by pouring about 4g of elastomer into the mould, followed by degassing in a vacuum chamber and curing at room temperature. When fully cured, the second elastomer was poured into the mould until full. Excess elastomer was removed with a metal scraper to level the samples and samples were cured at room temperature. Two batches of three samples were prepared, reversing the order in which the different elastomers were moulded (representative example shown in Figure 1)

Figure 1: Representative examples of samples for compression testing: Ecoflex 00-30 (left), moulded composite (middle) of Ecoflex 00-10 (blue) and Ecoflex 00-30 (white), and printed composite (right) of Ecoflex 00-10 (blue) and Ecoflex 00-30 (white).

Samples were compressed up to 4 mm displacement (~20-30% strain) at 12 mm/min (ASTM 575-91) using a mechanical materials testing system (Instron 5969) fitted with a 500 N load cell (2580-500N or 2530-500N, depending on availability). An initial test was carried out to remove the potential Mullins effect[1] from the samples. Data from the second test was used for the analysis of the material behaviour.

Several hyperelastic material models were then fitted to the averaged stress-strain data using Ansys 19.0 software, which will now be described.

Computational Modelling

We tested the quality of the fit of the material parameters that had been produced by ANSYS. A computational finite element model was created in FEBio that mirrored the material testing. This consisted of a rounded wedge-shaped geometry with predominantly second order hexahedral

elements (HEX20, n = 448) and second order pentahedral elements at the point (PENTA15, n = 64). Use of three symmetry planes allowed us to only model one eighth of the original material samples. The model had a radius of 14.3 mm, thickness of 6.25 mm, and angle of 90°.

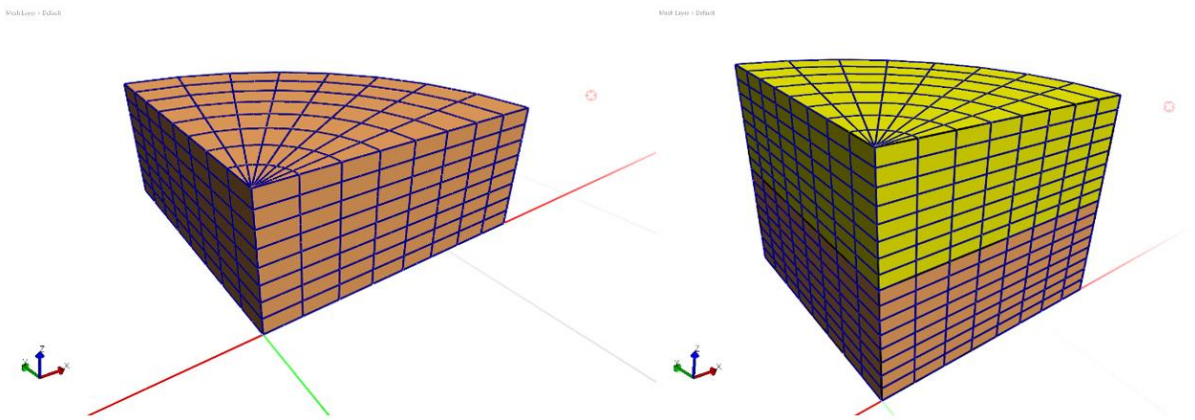

Figure 2: Visualisation of a) single material sample; b) composite material sample

Neo-Hookean and first order Ogden models were evaluated. Parameters for these models were derived from the model fits from the material testing and are presented in table 1.

Model	Parameters	DragonSkin 10	EcoFlex 00-10	EcoFlex 00-30	Smooth-Sil 950
Neo-Hookean	E	2.51E+05	3.83E+04	6.59E+04	1.64E+06
Neo-Hookean	v	0.49	0.49	0.49	0.49
1st Order Ogden	k	1.20E+08	1.64E+07	3.27E+07	7.76E+08
1st Order Ogden	c1	239876.5198	32879.4	65337.85	1551657
1st Order Ogden	m1	7.9319	5.6337	6.5892	9.1814

Table 1: Derived Parameters for a selection of tested silicones using Neo-Hookean and 1st Order Ogden Models

All nodes on the planes of symmetry were constrained to movements in their respective planes. The top surface of the model was then displaced down by 1.5 mm to give an equivalent sample compression of 3 mm.

A second model was created to show the behaviour of a composite with EcoFlex 00-10 and DragonSkin 10. This model had a 6.2 mm layer of DragonSkin 10 with a 6.0 mm layer of EcoFlex 0-10 on top.

Graded Printing

Gradient samples were printed using a Hydra 16A 3D printer (Hyrel, Inc.) with two SDS-30 print heads, featuring 30cc syringes, that fed the silicone into a SMH-2 mixing head (both from the same company). Ecoflex 10 (Smooth-On, Inc.) (A in Figure 3) and Ecoflex 30 (Smooth-On, Inc.) (B in

Figure 3) was each thoroughly mixed in a ratio of 1:1, dyed using silicone pigment (<1%, Silc Pig, Smooth-on, Inc) and degassed in a vacuum chamber.

The samples were printed into an aluminium mould of 28.6 mm diameter and 12.5 mm thickness (ASTM 575-91), which was fixated onto the print bed. Six layers with layer a layer thickness of around 2mm were extruded producing an overall 50/50 gradient structure from Ecoflex 10 to Ecoflex 30, as shown in figure 2. The samples were afterwards cured by room temperature and demoulded afterwards.

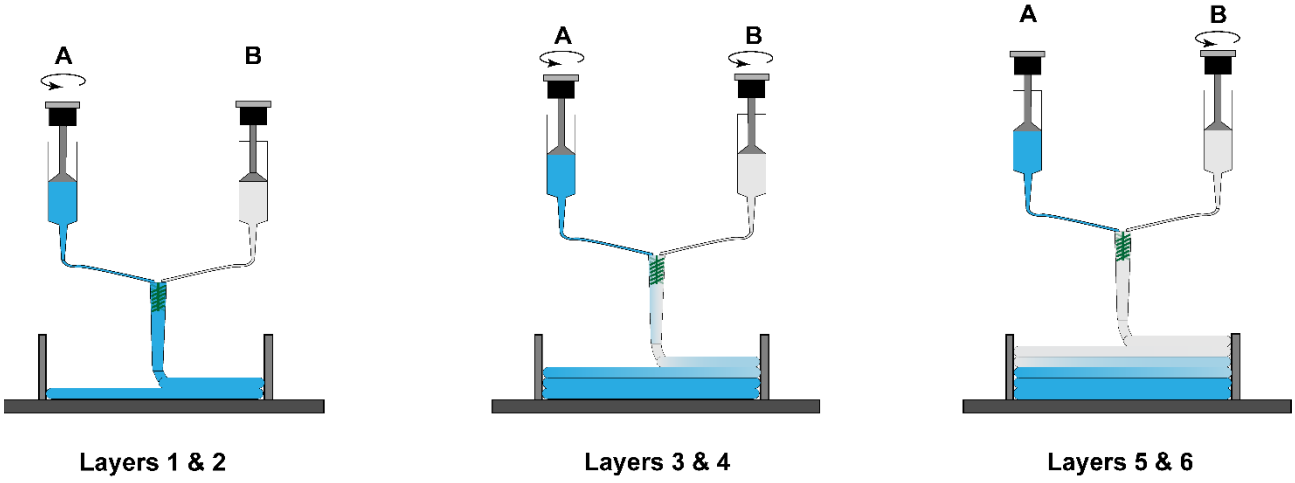

Figure 2: Diagram showing the iterative printing of the layers of 2 types of silicone

All samples were tested using the same methodology as described in section “Material Testing”, and are presented below, with an example print shown in Figure 3.

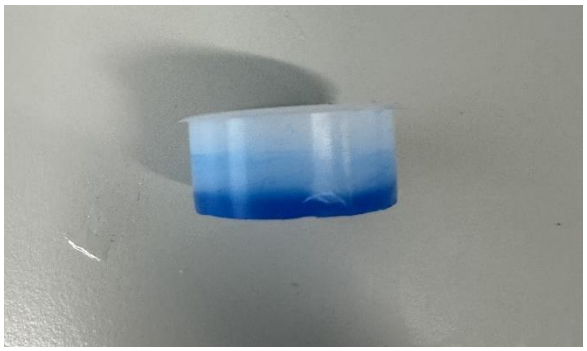

Figure 3: A composite graded print with Ecoflex 10 and Ecoflex 30

Device Scale Work

A new finite element model was developed, building upon a published methodology for transtibial amputation scenario [9], that extends this to an upper limb geometry, along with incorporation of a liner in the model for virtual testing.

Following the aim to generate a generic, parameterisable model, arm geometry was developed from the open-access published dataset presented in Kerkhof et al [10] which was generated from a 60-year-old male through the authors' university voluntarily human body donation programme. As such, no further ethical approval was necessary for the present study. By making an approximate segmentation of the bones in the MR images, the soft tissue surface mesh was aligned with the accurate CT-based bone models by rigid registration. Finally the soft tissue and bone meshes were virtually amputated by applying a planar cut approximately transverse to the forearm's long axis and a surface-tangent closure, in Meshmixer (Autodesk Inc., CA, USA). A uniform thickness offset and proximal planar cut were applied to the soft tissue external surface body to generate a simplified liner body.

Finally, the liner external surface mesh was duplicated and modified to represent a simplified socket, according to published design features [11,12]. First, in Meshmixer the shape was trimmed proximally and flared to produce a brim, and then local supracondylar and olecranon bar rectifications were applied. Then in a Python environment a linearly increasing radial press-fit was applied by repositioning the mesh vertices, and the distal end extended.

The irregular anatomic body .stl meshes were meshed in ANSYS with 2nd order tetrahedral elements, and the mesh converted into .inp format. A mapped 2nd order hexahedral mesh was generated on an idealised cylindrical liner model in ABAQUS, which was then morphed onto the residual limb model using non-rigid Iterative Closest Point (ICP) matching [13] and a radial basis function (RBF) method [14], coded in Python. The socket was map-meshed with 2nd order quadrilateral shell elements. The meshes were compiled into .inp format and imported into FEBio [15] for further pre-processing and solution. According to the previously published transtibial methodology [9] linear elastic material properties were assigned to the bone and socket, and compressible neo-Hookean properties were assigned to the collected soft tissues and liner (Table 2) according to the following strain energy function:

$$\psi = C1I1\text{-}3 + 12K\ln J\ 2$$

The limb-liner interface was assigned a tied contact, and sliding contact with a 0.5 coefficient of friction was assigned at the liner-socket interface.

Structure		
Bone (Linear Elastic)	E = 12,000 MPa	v = 0.3
Soft Tissue (Neo-Hookean)	C = 8.075 kPa	D = 1.243 MPa^{-1}
Liner (Neo-Hookean)	C = 37.6 kPa	D = 0.54 MPa^{-1}
Socket (Linear Elastic)	E = 1,500 MPa	v = 0.3

Table 2: Assigned material properties

Fixed displacement boundary conditions were applied at the model's proximal cut surfaces. The socket was displaced along the approximated forearm axis into a position of nominal initial contact, and then moved onto the limb by applying a fixed displacement to a control point at the centre of the distal connector tube, to represent donning A variety of load cases are being tested one by one, representing simplified ADL scenarios, with a variety of results metrics intended to corroborate the

model by comparison to published data (Table 3), and the model will be solved, with these results expected soon.

Load Case	Description	Results Metrics
A) Tip loading for socket coupling in flexion-extension	22.2N (5lbf) force applied to socket tip at 45° to residual forearm axis, in the sagittal plane [10]	Relative radius-socket axis rotation in sagittal plane Socket-Liner interface pressure Soft tissue Lagrangian strain
B) Push loading along residual limb axis, for socket axial coupling	TBC	Relative radius-socket axial displacement Socket-Liner interface pressure Soft tissue Lagrangian strain
C) Load Carrying / Doffing	Socket displaced distally through socket connector tube centre until doffed.	Peak reaction force

Table 3: Load Cases and Results Metrics

Fabrication and Repair

A technology transfer workshop was organised with Operation Namaste, and a tested mould based fabrication process was taught be Jeff Erenstone, CEO and Certified Prosthetist from their team. This means moving forward with a high quality method that is available to our lab for future work.

Some highlights from that process are shown in Figure 4:

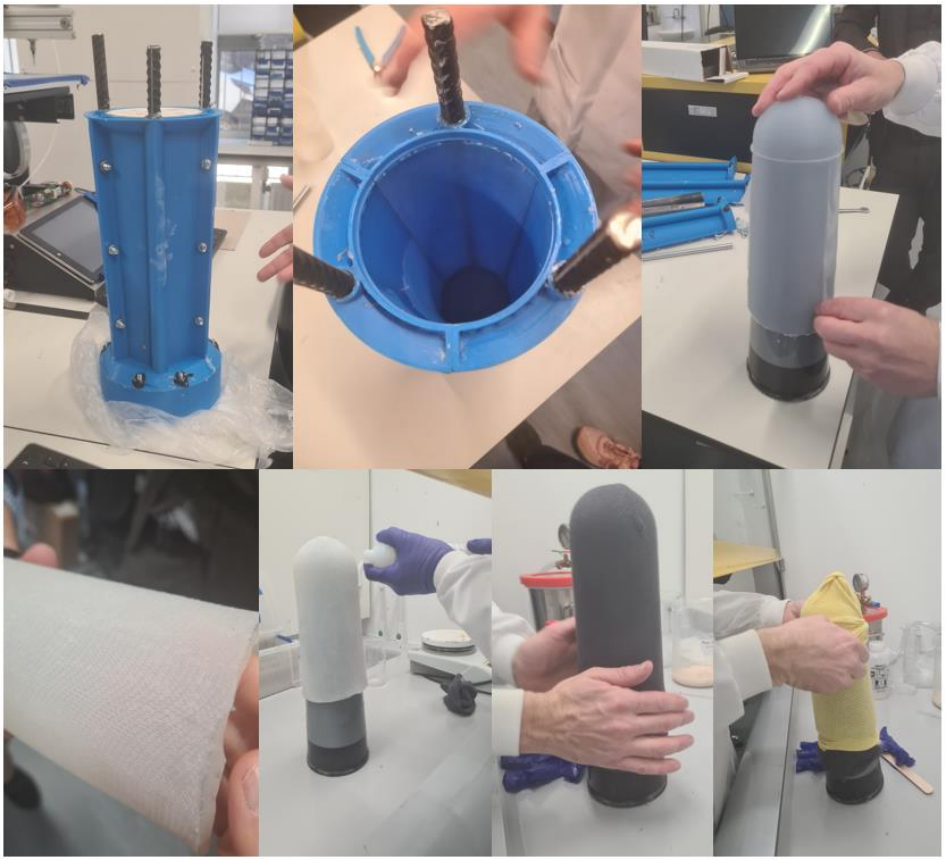

Figure 4: Liner fabrication workshop facilitated by Operation Namaste

An upper residual limb model geometry based on the open access published dataset presented in Kerkhof et al. [2] seen in Figure 5 was converted into a four part mold, based on the Operation Namaste mould, but consisting of two side parts, a bottom and top part using commercially available CAD software.

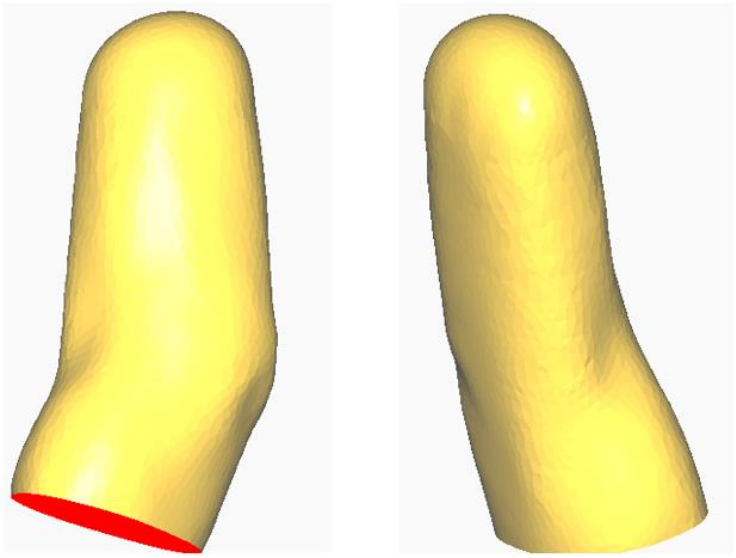

Figure 5: The upper residual limb model geometry based on the open access published dataset presented in Kerkhof et al. [2], with a virtual amputation as discussed above for the modeling

The parts were 3D printed using an Ultimaker S5 (Ultimaker Ltd.), using white PLA filament from the same company. This can be seen in Figure 6.

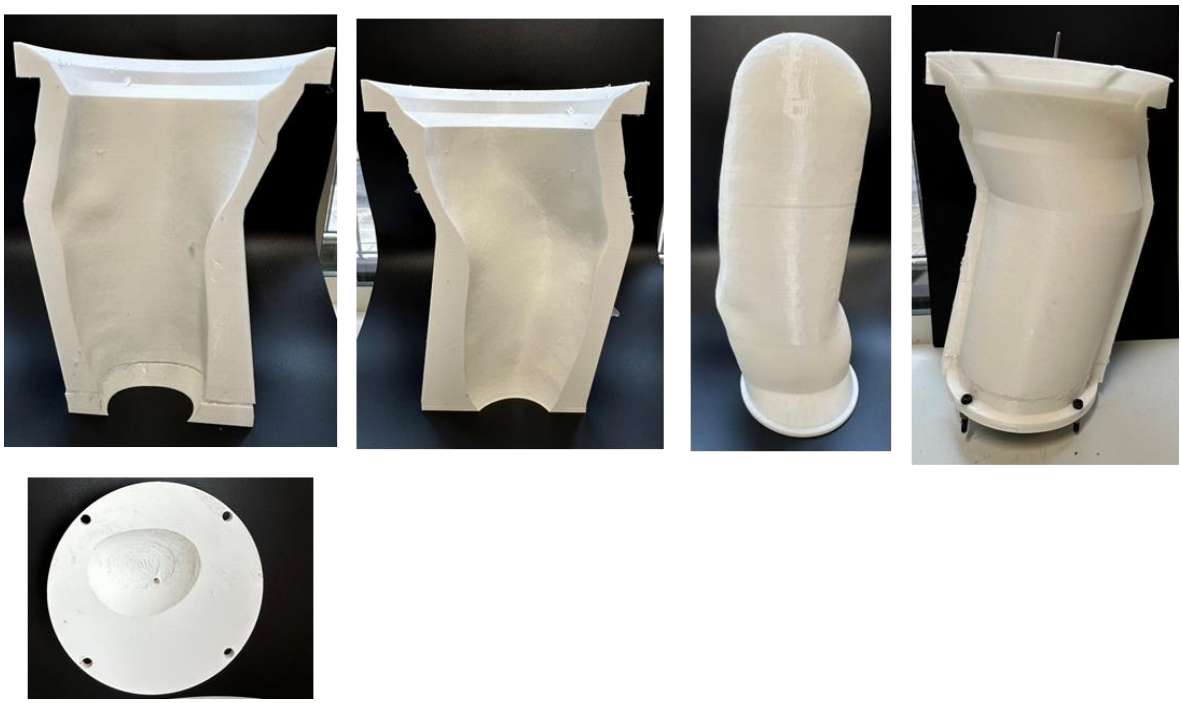

Figure 6: Custom mould sections for an upper residual limb

The mould was assembled and sprayed with Silicone release agent Ambersil (CRC Industries UK Ltd). Elastosil 3837/60 A/B (Wacker Chemie AG) was mixed in a ratio of 1:1 (A:B) and thoroughly mixed and degassed using a vacuum chamber. The mixture was poured into the mould and let to cure for 24 hours at room temperature. The liner was de-moulded and inspected for tears and holes.

Damage Investigation and Repair Strategy Development for Liners

Prior to repair a suitable cleaning strategy is needed. Used liners were cleaned by soaking in a Decon 90 (~3wt%, Decon) and water solution for 18-24 hours. Liners were thoroughly rinsed under a running tap to remove residual Decon 90. Damage on the liners was identified by optical inspection and damaged areas were cut out using scissors. The damaged patches were further investigated using optical microscopy (Keyence VHX-7100) including topography analysis.

Using the standard production ON moulds, we aimed to replicate the damage seen in the microscopy images, in a very rough manner using various implements to create different damage patterns. These are also meant to replicate larger damage known to be seen in used liners such as large tears. These large tears are assumed to be the longer term result of the microtears shown in microscopy images, however this is to be investigated in later studies, along with highly damaged used liners being used in place of replicated damage. This will also then test for repair of true biochemical/chemical/environmental damage that occurs in liners.

This replica damage was applied to an inverted moulded ON liner in the following patterns at different locations on the liner:

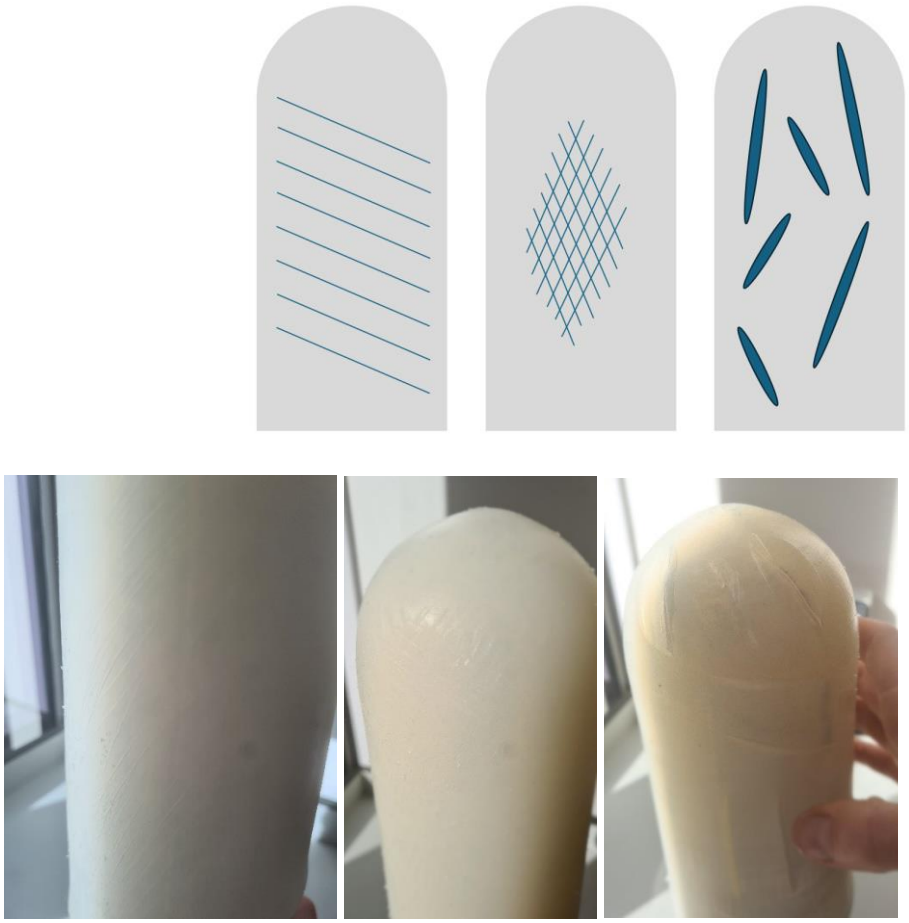

Figure 7: Damage applied to liner to simulate use

The damaged liner was then turned back to inside in and ‘remoulded’, with 50ml silicone poured into the liner, and mechanically applied to the whole inner surface with a spatula. The inner mould piece was then placed back in the mould and screws tightened to seal the liner in to the correct position and wall thickness and left to cure. The compression of the liner due to the addition of the fabric wall is noted compared to the original moulding of the silicone layer of the liner.

What we found

Material Testing for single layer, double layer and graded samples

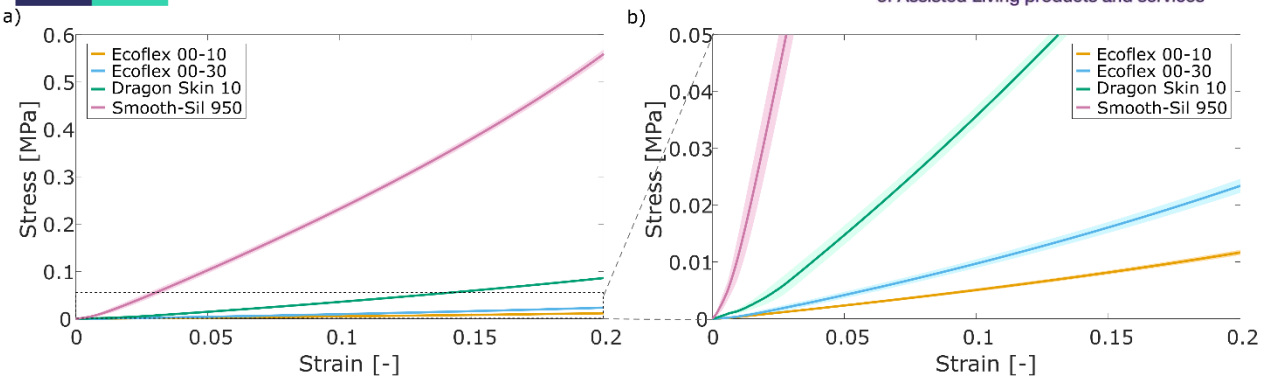

Figure 9: Compression results for four different elastomers: a) entire test; and b) zoomed-in on low stress regime. Shaded areas indicate the standard deviation, n=6 for all tests.

8 shows the compression behaviour for the four tested elastomers. The results indicate that Smooth-Sil 950 is the stiffest elastomer, and Ecoflex 00-10 is the softest. This finding is in line with the manufacturer's data, which provides limited information regarding the stiffness of these materials (e.g. 100% tension modulus). The detailed stress-strain behaviour from these tests, can provide better predictions about the material behaviour. Different material models were fitted to the experimental data to use in the numerical models. The comparison between the experimental and numerical models is covered in the 'Computational modelling' section.

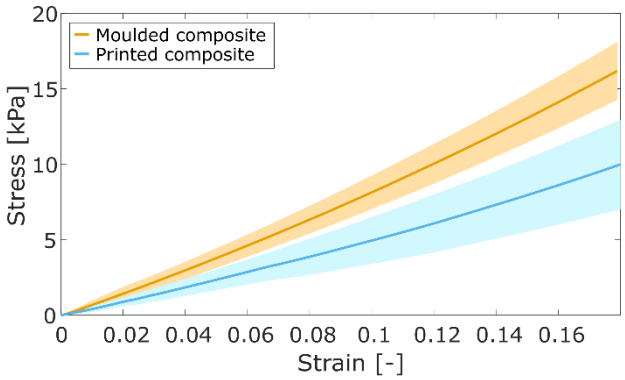

Figure 9: Stiffness comparison between moulded and printed composite samples. Shaded areas indicate the standard deviation, n=6 for moulded composite, n=5 for printed composite.

Figure 9 shows the comparison between the moulded and printed composite samples of Ecoflex 00-10 and Ecoflex 00-30. The graph indicates that the moulded samples have a higher average stiffness than the printed composite samples. One printed sample was excluded from the test results as the print did not meet the test samples specifications (<12 mm thickness). One potential explanation for the lower stiffness in the printed composite is a higher content of the softer elastomer (Ecoflex 00-10). Visual inspection of the samples did not convincingly support this hypothesis as the samples show an approximately 50/50 colour profile. The printed composites were not degassed prior to printing, which could trap air bubbles in the samples. The average density of the moulded and printed samples was, however, similar (<10% difference), which makes significant air entrapment an unlikely explanation for the observed stiffness difference. We will explore if similar stiffness differences occur in printed and moulded samples made from a single elastomer and if any step in the printing process may inhibit fully curing of the elastomers.

Computational Modelling

Figures 10 show the engineering stress-strain curve for the finite element model with Neo-Hookean (orange) and 1st Order Ogden (red) models. The plots compare these outputs from the finite element model to the stress-strain data from the material testing. There is a very good fit between the Ogden model the experimental results. The Neo-Hookean is not as good of a fit; this was already observed when the model parameters were fitted to the material testing data in ANSYS.

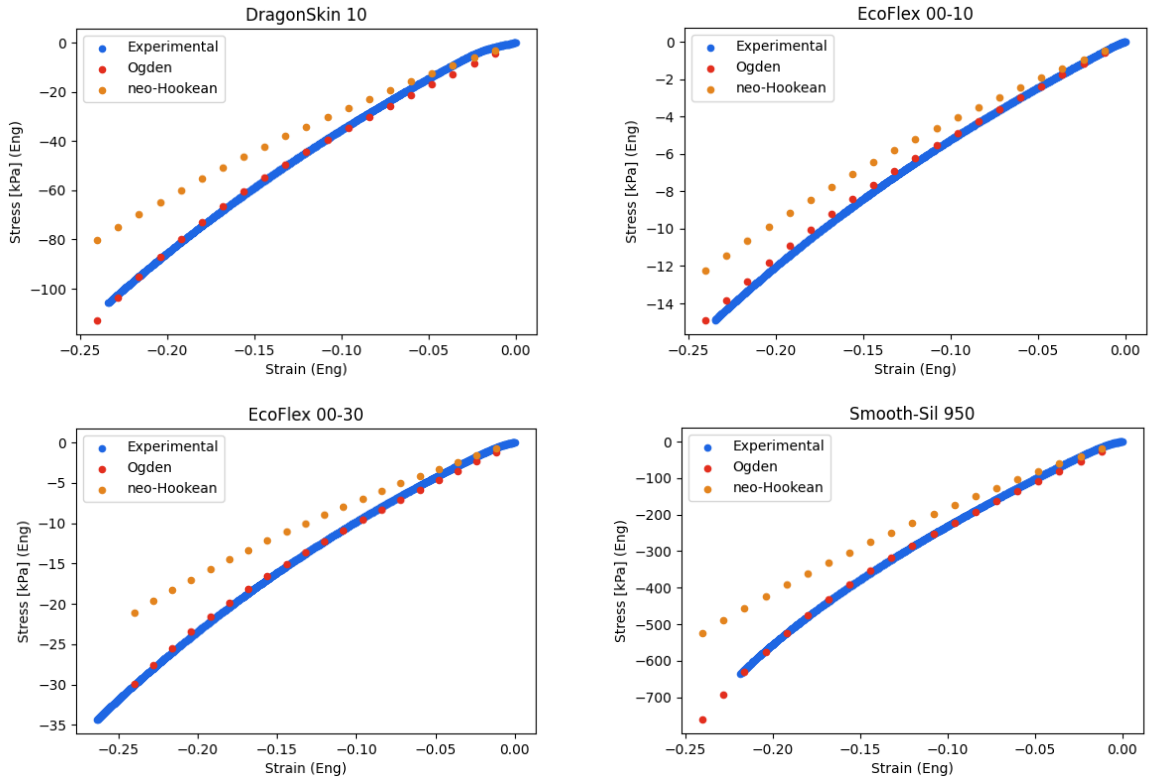

Figures 10: Engineering stress-strain curve for the finite element model with Neo-Hookean (orange) and 1st Order Ogden (red) models

Figure 11 shows the deformation of the composite sample with upper section modelled as EcoFlex 00-10 and lower section modelled as DragonSkin 10. The corresponding effective stress and strain figures 12 & 13 show a concentration of stress and strain at the interface between the two materials. This could contribute to delamination of the two materials. Having a gradual change in the material through the thickness may work to alleviate these stress concentrations and reduce the likelihood of damage. The overall engineering stress-strain behaviour of the composite finite element model matches well with the experimental compression tests (Figure 14).

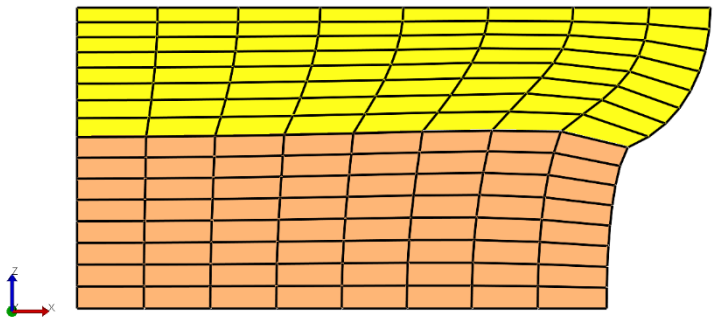

Figure 11: Deformation of the composite finite element model.

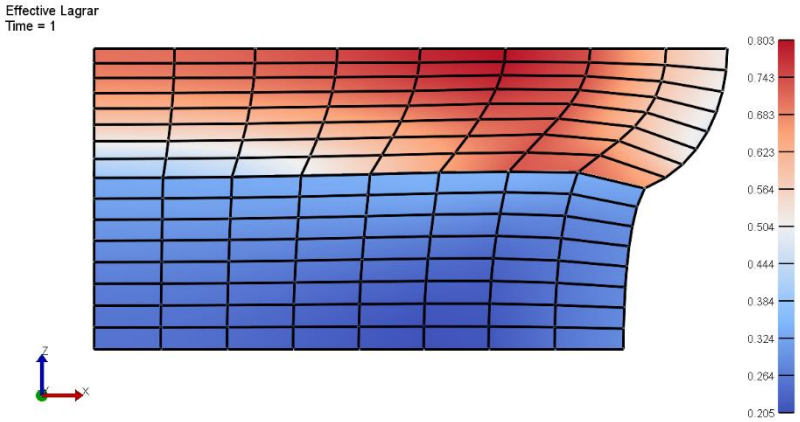

Figure 12: Strain distribution in the composite finite element model

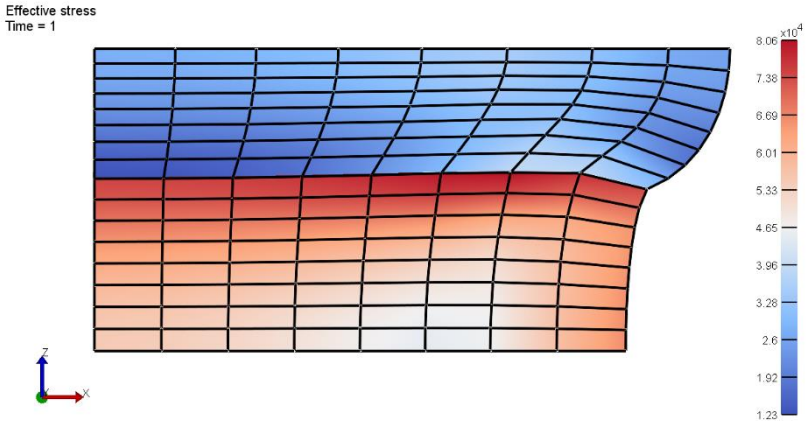

Figure 13: Stress distribution in the composite finite element model

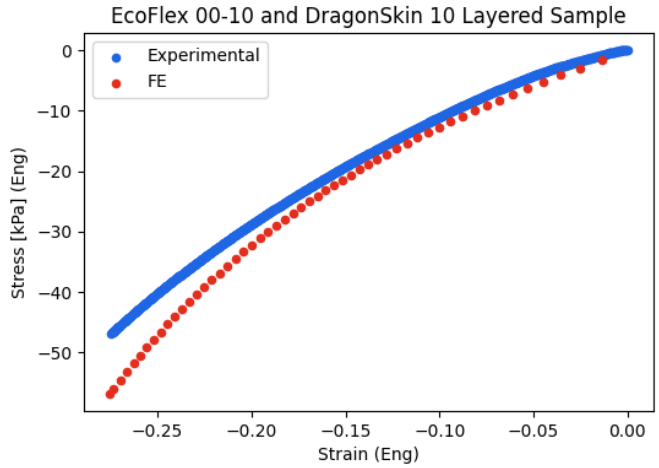

Figure 14: Stress-strain response of composite finite element model compared to experimental results

Device Scale Work

The Upper limb model is constructed, with visual highlights in Figure 15, results for load cases are the next step, prior to publication for this workstream.

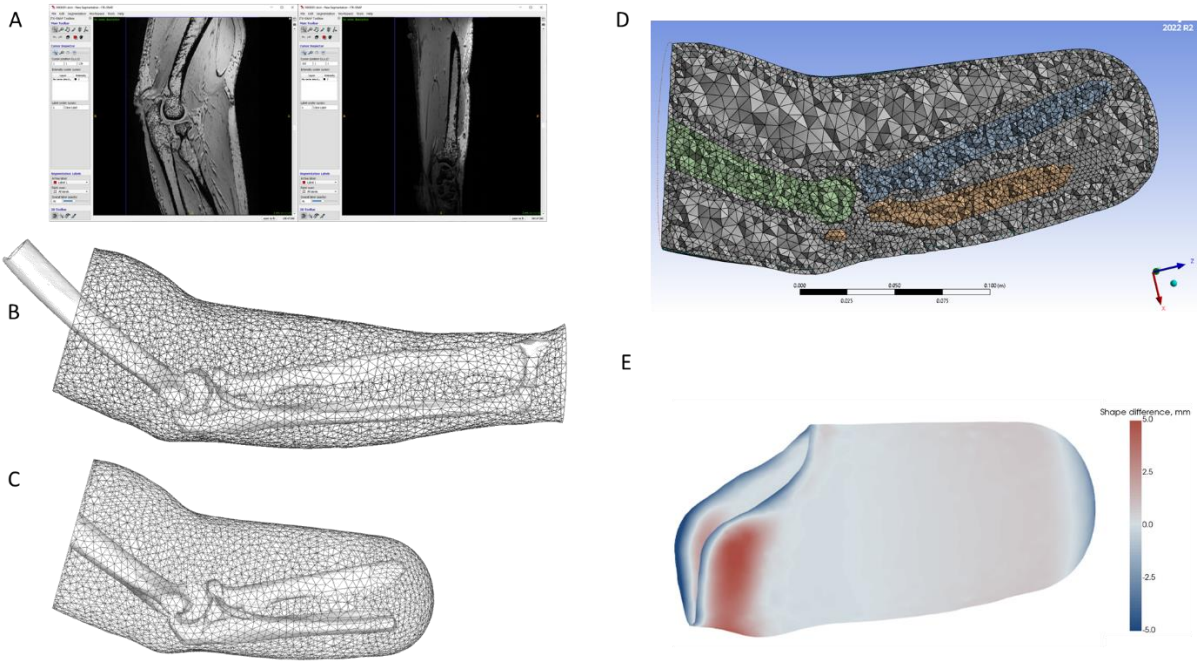

Figure 15: Model generation process from A) MRI data segmentation and surface meshing, B) limb surface mesh registration to bone models, C) virtual surgery, D) finite element meshing and E) socket rectification design.

Custom Liner Fabrication

In Figure 16 can be seen the silicone layer after curing. Testing of the application of the fabric layers are now being tested.

Figure 16: Inner silicone layer for custom liner. Testing of fabric layer construction will now proceed

Damage Investigation and Repair Strategy Development for Liners

Figure 17 highlights the different regions investigated for damage in a used liner. The microscopy images (17 b-d) show that the undamaged part of the liner (area 1, 17b) presents a smooth surface, whereas damage on the liner (area 2 and 3, 17c and 17d respectively) presents as a rough surface. The surface roughness was further investigated (17e and 17f) with local peaks up to approximately 400 µm (17f).

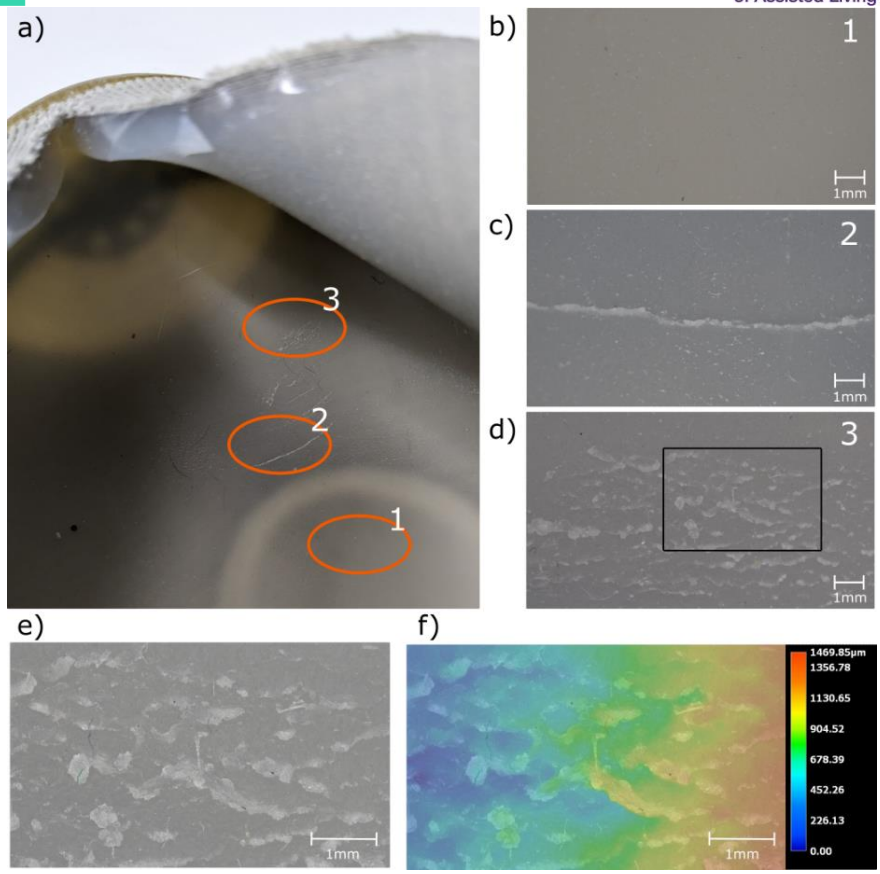

Figure 17: a) cut-open liner with three different locations identified for microscopy; b) location 1; c) location 2; d) location 3, with black rectangle identifying the area for a topography profile; e) microscopy image of highlighted area in d); f) topography profile of highlighted area in d).

The remoulded liner once cured was removed from the mould, which can be seen in Figure 18 below.

Figure 18: A repaired liner using a novel remoulding technique

On visual and tactile inspection, the removed liner appears as completely damage free, with zero visible or identifiable edges or subsurface interfaces between original and repaired areas. A method for non-destructive testing is needed for further validation of this technique, but this preliminary result shows great promise and justifies further investigation.

What this means

- The Ogden based model has shown good fit with experimental results, meaning further expansion of model-based physical testing can be taken forward with confidence.
- Damage to used liners exhibits a range of different modalities – investigating their nature could inform future repair vs maintenance strategies
- Remoulding of damaged liners has potential as a strategy, requiring very minimal use of additional silicone
- A upper limb model has been constructed and will be viable for virtual testing of UL socket-liner-limb interactions for a broad range of study.
- A tested moulded fabrication approach has been taught to our team that will enable mould-based experimentation on liner designs moving forward.

Rapid Liquid Printing in Substrate bath (Extension Project Work)

The 3D printing of liquid materials, such as silicones, resigns or foams, into substrate baths is widely known as liquid rapid printing (RLP). Printing into substrate baths allows the production of more complex 3D geometries, such as prothetic liners, as opposed to printing in a 2D plane.

We utilised the existing Hyrel 16A Liquid 3D printer (Hyrel Inc.) with SDS-30 print heads and equipped the print heads with a standard-size disposable 30cc syringe and standard-size disposable needle ranging from gauges 12G to 27G (Fisher Scientific Inc.) shown in Figure 19. For the printed material we chose Ecoflex-30(smooth-On Inc.), mixing each part at a ratio of 1:1, dying it using silicone pigment (<1%, Silc Pig, Smooth-On Inc) and degassing it in a vacuum chamber before filling the syringe. For the supportive bath we used Carbomer-940 powder (Myoc Cosmetics Ltd.) mixed with distilled water at a ratio of 1,2wt% Carbomer to water. Thoroughly mixing the substrate for a couple of minutes and adding 0.1wt% NaOH (Fisher Scientific Inc.) to produce gelling. The gel is then degassed in a vacuum chamber until all bubbles disappear and the gel is then sealed and stored.

The printer was setup as described above, and different needle gauges tested on a line-shaped test

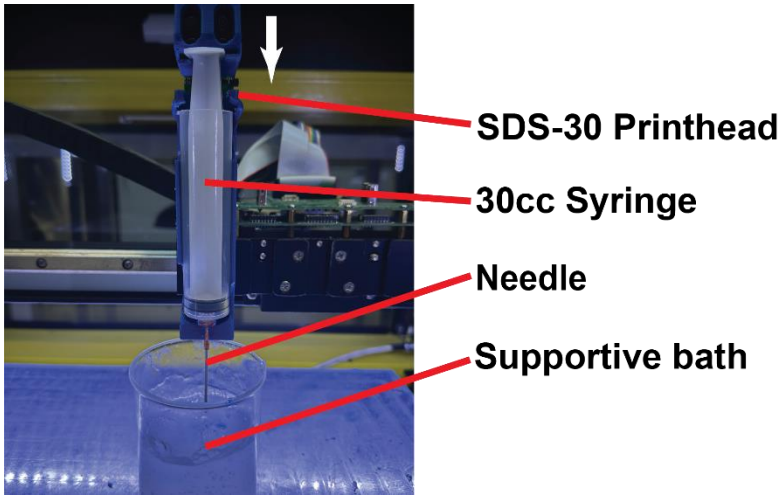

Figure 29 RLP setup using the Hyrel 16A 3D printer with an SDS-30 print head

sample. The flow percentage adjusted between 25% and 100% and the resulting print was assessed according to the criteria shown in Figure 20. The extruded line sample was either classed as “Not continuous” or “under extruded” when the resulting print was significantly lower (>20%) than

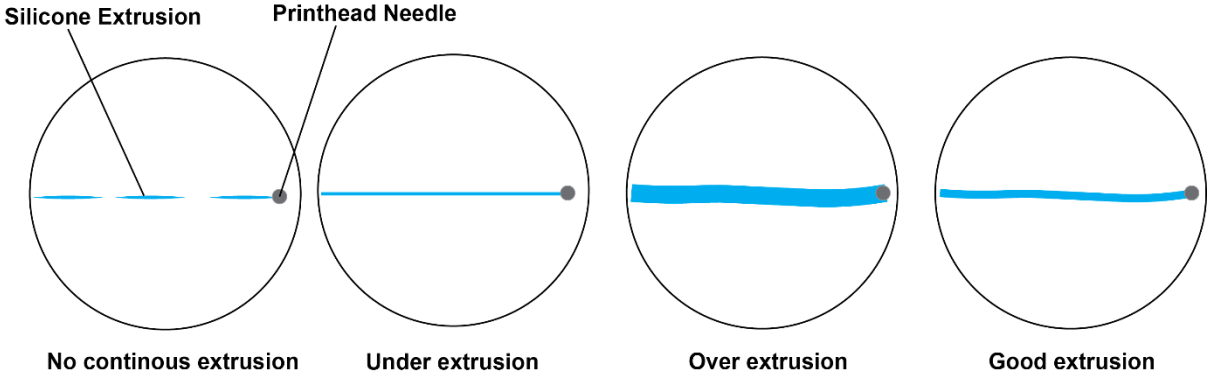

Figure 30 Ranking criteria for the extrusion of a simple line geometry comparing different needle gauge and flow percentages

Needle gauge and as “over extruded” when bigger (>20%). The classification of the extrusion was done by observation.

The tests as outlined in Table 4 showed that prints performed best with needle gauges 16G and 18G. Lower gauge needles (14G and 12G) printed well however they tended to over extrude at higher flow percentages. However, lower gauges allowed for larger flow rates of materials, as the extrusion width increases, resulting in faster prints. This can also be useful when considering bigger prints, as the

curing time for silicone printing materials, such as Ecoflex 30, is below 1hr, reducing the possible printing time. Higher needle gauges showed limited functionality under these methods resulting either in under extrusion or spotted extrusion. This could be in part a result of the viscosity of the silicone material, resulting to shear forces in the needle walls. Higher viscous printing materials might perform better print results using these higher gauge needles.

		Flow percentage			
		25%	**50%**	**75%**	**100%**
Needle Gauges	**12G**	Good Extrusion	Over extrusion	Over extrusion	Over extrusion
	14G	Good Extrusion	Over extrusion	Over extrusion	Over extrusion
	16G	Good Extrusion	Good Extrusion	Good Extrusion	Good Extrusion
	18G	Good Extrusion	Good Extrusion	Good Extrusion	Good Extrusion
	19G	Over extrusion	Over extrusion	Good Extrusion	Good Extrusion
	22G	Over extrusion	Over extrusion	Over extrusion	Over extrusion
	25G	No continous extrusion	No continous extrusion	Over extrusion	Over extrusion
	27G	No continous extrusion	No continous extrusion	No continous extrusion	Over extrusion

Table 4 Comparison of print extrusion of a simple line geometry with different flow percentages and needle gauges

After determining the appropriate needle gauge and adjusting print flow parameters, a simple 3D vase design was printed to evaluate whether modifications to the layer height were necessary, as well as to assess whether the layers effectively merged to form a continuous part. Figure 21 compares the sliced 3D model with the final printed sample. It is evident that the printed component exhibits strong interlayer adhesion, with minimal layer visibility. This observation indicates a high degree of fusion between the silicone layers, resulting in a uniform surface finish. However, due to the gel structure of the supportive bath, a movement of layers in the X-Y direction was observed which resulted in layers being slightly off centre for the final part. This could be resolved by diluting the gel bath to a higher viscosity using buffer solution.

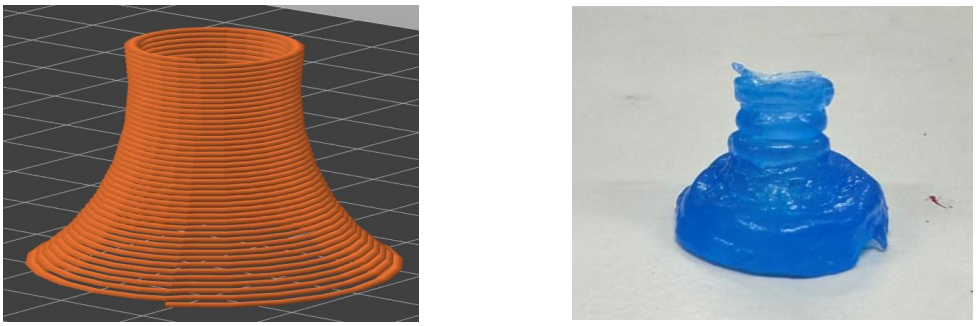

Figure 21: Comparison of Sliced geometry (left) with printed sample (right) of a vase like structure

We further examined the potential for generating infill using the slicer software's infill settings while fabricating a standard ASTM 575-91 compression disk, with infill percentages ranging from 25% to 100%. Lower infill gradients (up to approximately 60–70%) yielded reliable parts, with layers printing consistently as previously described. However, when using infill percentages exceeding 80%, the infill became overly dense and led to noticeable bulging of the final component, as depicted in Figure 22.

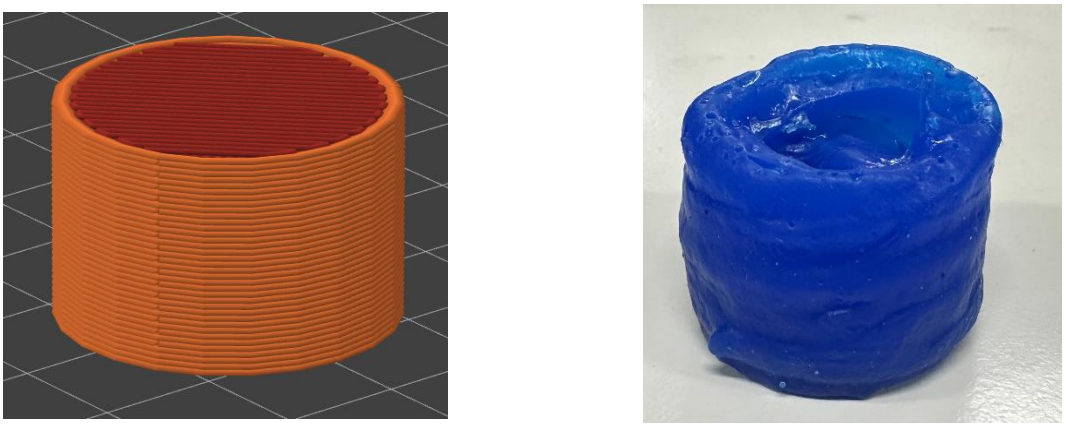

Figure 22 Comparison of Sliced geometry (left) with printed sample (right) of a ASTM 575-91 compression disk

In conclusion, rapid liquid printing (RLP) of basic geometries demonstrates considerable promise as a manufacturing approach for prosthetic liners, offering the potential to produce full-scale liners at relatively low-cost using silicone-based 3D printing. Nevertheless, additional investigation is required to develop efficient, high-detail RLP employing Ecoflex-30 silicone in a Carbopol 940 substrate. In particular, the interplay among needle gauge, flow rate, and layer height is critical for achieving high-quality prints. Moreover, the exploration of multi-material RLP is an exciting avenue for future work, as it could enable the fabrication of full-scale liner materials with gradient structures.

What next

- Load case results for the UL model and write up in journal Paper outlining the development and results
- Remoulding repair strategy will be tested with 13 users on used liners coming back from Operation Namaste Study
- Journal Paper outlining the material patch testing vs patch modelling
- More detailed materials testing using strain tracking with camera setup – other work focusses mostly on tensile testing. Publication with detailed compressive data + material models contribution to soft materials literature (relevant for prosthetics, orthotics, soft robots etc.).
- EP applied for a Royal Academy of Engineering (RAEng) Research Fellowship, proposing a research project with BO and AD as collaborators that builds on the work on composite

liners, custom liner design, liner printing, and computational liner modelling. Her proposal was put forward by UCL after a rigorous internal selection (15% success rate) to be submitted to the RAEng. She is invited for an interview as part of the last stage (of a three-stage process) of the RAEng selection process. If successful, EP receives 5 years of personal funding (850k+ FEC), plus 2 PhD studentships.

- User testing of graded material for comfort against skin
- Pilot Study on custom liner production with a UK lower limb prosthesis user
- Further refinement of the rapid liquid printing approach

References

1. Rohwerder, B. *Assistive Technologies in Developing Countries*; Institute of Development Studies: Brighton, UK, 2018. [Google Scholar]

2. Oldfrey, B.; Barbareschi, G.; Morjaria, P.; Giltsoff, T.; Massie, J.; Miodownik, M.; Holloway, C. Could Assistive Technology Provision Models Help Pave the Way for More Environmentally Sustainable Models of Product Design, Manufacture and Service in a Post-COVID World? *Sustainability* 2021, *13*, 10867. https://doi.org/10.3390/su131910867

3. G.K. Klute, B.C. Glaister, J.S. Berge Prosthetic liners for lower limb amputees: A review of the literature Prosthetics and Orthotics International, 34 (2) (2010), pp. 146-153, 10.3109/03093641003645528

4. Oldfrey B, Tchorzewska A, Jackson R, Croysdale M, Loureiro R, Holloway C, Miodownik M. Additive manufacturing techniques for smart prosthetic liners. Med Eng Phys. 2021 Jan;87:45-55. doi: 10.1016/j.medengphy.2020.11.006. Epub 2020 Nov 13. PMID: 33461673.

5. Steer JW, Worsley PR, Browne M, Dickinson AS. Predictive prosthetic socket design: part 1-population-based evaluation of transtibial prosthetic sockets by FEA-driven surrogate modelling. Biomech Model Mechanobiol. 2020 Aug;19(4):1331-1346. doi: 10.1007/s10237-019-01195-5. Epub 2019 Jun 29. PMID: 31256276; PMCID: PMC7423807.

6. Steer JW, Grudniewski PA, Browne M, Worsley PR, Sobey AJ, Dickinson AS. Predictive prosthetic socket design: part 2-generating person-specific candidate designs using multi-objective genetic algorithms. Biomech Model Mechanobiol. 2020 Aug;19(4):1347-1360. doi: 10.1007/s10237-019-01258-7. Epub 2019 Nov 18. PMID: 31741116; PMCID: PMC7423857.

7. https://www.ossur.com/en-ca/professionals/orthotic-and-prosthetic-services/ossur-legs/custom-liners

8. Diani, Julie, Bruno Fayolle, and Pierre Gilormini. "A review on the Mullins effect." *European Polymer Journal* 45.3 (2009): 601-612.

9. Steer, J.; Worsley, P.; Browne, M.; Dickinson, A. Key considerations for finite element modelling of the residuum-prosthetic socket interface. *Prosthet. Orthot. Int.* **2021**, *45*, 138–146.

10. Kerkhof, F.D.; van Leeuwen, T.; Vereecke, E.E. The digital human forearm and hand. *J. Anat.* **2018**, *233*, 557–566, doi:10.1111/joa.12877.

11. Miguelez, J.M.; Lake, C.; Conyers, D.; Zenie, J. The Transradial Anatomically Contoured (TRAC) Interface: Design Principles and Methodology. *J. Prosthetics Orthot.* **2003**, *15*, 148–157, doi:10.1097/00008526-200310000-00007.

12. Ngan, C.; Pendse, V.; Sivasambu, H.; Ouellette, E.; Ready, N.; Andrysek, J. Preliminary Characterization of Rectification for Transradial Prosthetic Sockets. *Sci. Rep.* **2024**, *IN PRESS*.

13. Amberg, B.; Romdhani, S.; Vetter, T. Optimal Step Nonrigid ICP Algorithms for Surface Registration. In Proceedings of the IEEE Conference on Computer Vision and Pattern Recognition; 2007; pp. 0–7.

14. Zhang, J.; Ackland, D.; Fernandez, J. Engineering Point-cloud registration using adaptive radial basis functions. *Comput. Methods Biomech. Biomed. Engin.* **2018**, *21*, 498–502, doi:10.1080/10255842.2018.1484914.

15. Maas, S.A.; Ellis, B.J.; Ateshian, G.A.; Weiss, J.A. FEBio : Finite Elements for Biomechanics. *J. Biomech. Eng.* **2012**, *134*, 1–10, doi:10.1115/1.4005694.

Appendix 1

Carbon calculations for travel undertaken as part of the project

None